Manipulating photonic signals by a multipurpose quantum junction

M. Ahumada [1,*] P. A. Orellana [1,†] and A. V. Malyshev [2,3,‡]

[1] *Departamento de Física, Universidad Técnica Federico Santa María, Casilla 110 V, Valparaíso, Chile*

[2] *GISC, Departamento de Física de Materiales, Universidad Complutense, E-28040 Madrid, Spain*

[3] *Ioffe Physical-Technical Institute, 26 Politechnicheskaya str., 194021 St. Petersburg, Russia*

(Received 7 March 2022; accepted 22 March 2022; published 6 April 2022)

We address a prototype integrated quantum circuit model system: a multifunctional quantum junction comprising three-level atomic nodes that couple two waveguides. We consider nodes with the Λ scheme of the allowed optical transitions, one of which is driven by an external classical electromagnetic field. We demonstrate that the latter field can be used to control the mode of the device operation: studying the dynamics of optical pulses, we show that the proposed integrated junction can operate as a controlled router or a switch, a 1/4 splitter, a delay line, or a storage node. The system offers also a possibility of intrinsic parallelism of quantum operations and can provide useful guidelines for making possible future quantum circuitry building blocks more scalable and integrated.

DOI: 10.1103/PhysRevA.105.043502

I. INTRODUCTION

The operation of modern networks relies on the functionality of rather complex key devices, such as switches, routers, repeaters or amplifiers, etc. The functionality of these devices is provided by combinations of elementary operations performed by much more basic elements, such as delay lines, memory cells, and simple routing nodes. Network technology and devices are well developed for the classical electronic networks, while they are still in an active research phase in the field of the quantum ones. In a quantum network, photons are believed to be the natural candidates for carrying information with high fidelity as flying qubits in long-distance communications over quantum channels [1–7]. Therefore, considerable effort has been put into studies of photon transport in waveguides coupled to quantum emitters [8–11]. These emitters can be coupled to the quantum channels not only to inject information carriers but also to manipulate and route them, controlling pathways of signals in the network. Routing is one of the most important operations in a network, for which reason various implementations of quantum routers has been proposed [12–28]. However, it would be advantageous if a single device could provide multiple fundamental functionalities: operating as a router, a delay line, a splitter, or an information storage node. Below we report on a prototype of such a multipurpose device: a quantum junction comprising three-level systems coupling two waveguides.

II. MODEL

Our proposed prototype setup comprises two waveguides, which are symmetrically coupled by an N sequential three-level system, as shown schematically in Fig. 1. In an optical system, such waveguides can be the coupled-resonator waveguides (CRW), i.e., one-dimensional arrays of optical cavities (see, for example, Ref. [29] and references therein). Several experimental realizations of CRWs have been reported [29–33], in particular, large-scale ultrahigh-Q coupled nanocavity arrays based on photonic crystals [30]. CRWs have been successfully modeled by a simple discrete tight-binding bosonic model [9,10,12–17,34,35], which we use in what follows. The two waveguides (labeled A and B) are modeled as one-dimensional arrays of sites described by bosonic operators $a_n^\dagger$ and $b_n^\dagger$, which create a photon with the energy $\hbar\omega_0$ at the nth site of the corresponding waveguide. Adjacent sites are coupled by the nearest-neighbor interaction constant ξ. For simplicity, we consider identical sites and identical three-level systems. We assume also that the latter are atoms with the Λ scheme of the energy levels comprising the ground $|g_j\rangle$, the excited $|e_j\rangle$, and the third state $|s_j\rangle$ (where j labels the atom, $j = 1 \ldots N$). Energies of these states are E_g, E_e, and E_s, respectively. The dipole-allowed transitions $|g_j\rangle \leftrightarrow |e_j\rangle$ are coupled to the modes $a_j^\dagger$ and $b_j^\dagger$ of the neighboring waveguide sites by the coupling constant g. Other allowed transitions $|s_j\rangle \leftrightarrow |e_j\rangle$ are driven by an external classical control field which has the frequency ω_c and the Rabi frequency Ω. Transitions $|g_j\rangle \leftrightarrow |s_j\rangle$ are dipole forbidden.

Within the rotating-wave approximation and in the rotating frame described by the partial Hamiltonian [35]

$$H_R = \hbar\omega_0 \sum_n (\hat{a}_n^\dagger \hat{a}_n + \hat{b}_n^\dagger \hat{b}_n) + \hbar\omega_0 \sum_j (|e_j\rangle\langle e_j| + |s_j\rangle\langle s_j|) - \hbar\,\omega_c \sum_j |s_j\rangle\langle s_j|,$$

*maritza.ahumada@usm.cl

†pedro.orellana@usm.cl

‡a.malyshev@fis.ucm.es

which incorporates all high-frequency components, the Hamiltonian of the system reads as

$$\begin{aligned} H = &-\xi \sum_n [\hat{a}_n^\dagger \hat{a}_{n+1} + \hat{b}_n^\dagger \hat{b}_{n+1} + \text{H.c.}] \\ &+ \sum_j [\Delta_e |e_j\rangle\langle e_j| + (\Delta_e - \Delta_s)|s_j\rangle\langle s_j|] \\ &+ \sum_j [g\,|e_j\rangle\langle g_j|(\hat{a}_j + \hat{b}_j) + \hbar\Omega |e_j\rangle\langle s_j| + \text{H.c.}], \end{aligned} \tag{1}$$

where $\Delta_e = E_e - E_g - \hbar\omega_0$ and $\Delta_s = E_e - E_s - \hbar\omega_c$ are the detunings of the photon energies from the two allowed transition energies [36]. Hereafter, we consider the resonant case $\Delta_e = \Delta_s = 0$; we also set $\hbar\omega_0$ as the reference energy level, the coupling constant ξ as the energy unit, and $\hbar = 1$. Each standalone waveguide supports plane-wave modes with the dispersion relation $E(k) = -2\cos k$, where $k \in [0, \pi]$.

To study the dynamics of a wave packet defined as $|\Psi\rangle = \sum_n [\alpha_n a_n^\dagger |g_n, 0\rangle + \beta_n b_n^\dagger |g_n, 0\rangle] + \sum_j [u_j |e_j, 0\rangle + v_j |s_j, 0\rangle]$, with $|0\rangle$ being the vacuum state of the waveguides, we use the time-dependent Schrödinger equation with the Hamiltonian (1) written for the amplitudes α_n, β_n, u_j, and v_j:

$$\begin{aligned} \dot{\alpha}_n &= i\,(\alpha_{n+1} + \alpha_{n-1}) - i\,g\,\delta_{nj}\,u_j, \\ \dot{\beta}_n &= i\,(\beta_{n+1} + \beta_{n-1}) - i\,g\,\delta_{nj}\,u_j, \\ \dot{u}_j &= -i\,\Omega\,v_j - i\,g\,(\alpha_j + \beta_j), \\ \dot{v}_j &= -i\,\Omega\,u_j, \end{aligned} \tag{2}$$

where δ_{nj} is the Kronecker symbol, $j = 1 \ldots N$, $n = -N_0 \ldots N_0 + N$, and N_0 is the number of sites in each of the left and right channels (branches) of the waveguides. For further reference, we label regions of the system as follows: left channels A_L and B_L (with $n = -N_0 + 1 \ldots 0$), the central region C (with n, $j = 1 \ldots N$), and right channels A_R and B_R (with $n = N + 1 \ldots N_0 + N$). We define also probabilities to find the wave packet in different channels and at the atomic states:

$$\begin{aligned} P_{AL,AR} &= \sum_{n \in A_{L,R}} |\alpha_n|^2, \\ P_{BL,BR} &= \sum_{n \in B_{L,R}} |\beta_n|^2, \\ P_C &= \sum_j |u_j|^2 + |v_j|^2. \end{aligned} \tag{3}$$

We solve the system (2) numerically using the following normalized Gaussian wave packet as the initial condition:

$$\begin{aligned} \alpha_n &= \frac{1}{\sqrt{\sigma\,\sqrt{\pi}}}\, e^{-\frac{(n-n_0)^2}{2\sigma^2} + i\,k_0 n}, \\ \beta_n &= u_j = v_j = 0, \end{aligned} \tag{4}$$

where $\sigma, k_0 > 0$, and n_0 are the width, the wave vector, and the initial position of the center of the wave packet, respectively. Such a wave packet is propagating from left to right in the A_L channel. We always choose $n_0 = -[N_0 - 3\sigma]$, so that the amplitude of the wave packet at the connected region C is negligible at $t = 0$.

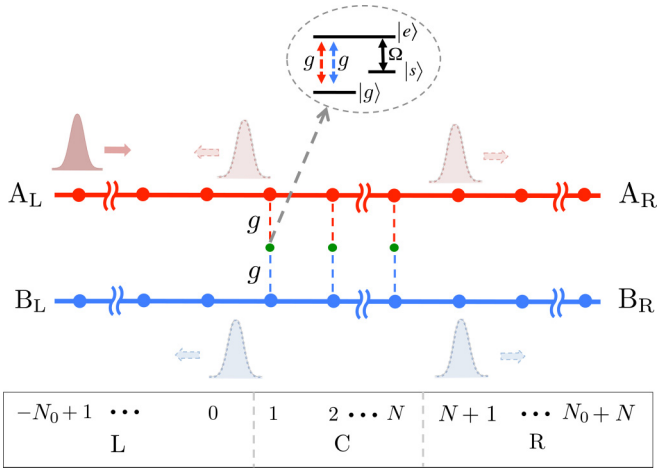

FIG. 1. Schematics of the system comprising two channels A and B which are coupled by N three-level Λ atoms. The diagram of the atomic energy levels and transitions is shown in the inset (see text for details). The left, coupled, and right regions of the system are labeled by letters L, C, and R, respectively. Also shown schematically is an incident wave packet propagating from left to right in the input branch A_L; the packet can be partially reflected back and partially transmitted into the output branches A_R, B_L, and B_R. All branches have the same number of sites N_0.

Hereafter, we consider the system with $N_0 = 1000$, $N = 12$, and $g = 0.5$. Such a system was studied in Ref. [35], where it was demonstrated that it has promising scattering properties in the stationary regime for certain sets of parameters. Below, we address the dynamics of wave packets for the most relevant parameter sets.

III. ROUTING EFFECTS

First, we investigate the system in the regime of controlled routing: we show that a wave packet incoming from the left input channel A_L can be routed into one of the two right output channels, A_R or B_R, which can be selected by the control field Ω. To this end, we analyze the stationary spectra of the transmission into the two right output channels, T_{AR} and T_{BR}, for two different values of the control field: $\Omega = 0$ and $\Omega = 0.85$ (see Ref. [35] for details of their calculation); the spectra are shown in panels (a) and (b) of Fig. 2, respectively. These spectra have useful features in the vicinity of $E_0 \approx 0.48$, i.e., the high and low values of the transmission probabilities into the output channel A_R or B_R can be swapped when the control field is switched from $\Omega = 0$ to $\Omega = 0.85$ or vice versa. Then, almost the whole wave packet can be routed into one or the other output channel under the following conditions: (i) the incoming wave packet is properly centered at $E_0 \approx 0.48$ and (ii) its width in the energy space ΔE is smaller than the width of the transmission features ($\approx$0.1).

To demonstrate the feasibility of such routing, we consider the dynamics of the wave packet centered at $k_0 = \arccos(-E_0/2) \approx 1.33$ and having the width $\Delta E = 0.02$ in the energy space (which is much smaller than the width of the above-mentioned spectral features). The corresponding wave-packet width in the real space σ can be estimated as $\sigma = 2\sin k_0/\Delta E \approx 100$. The dynamics of such a wave packet for

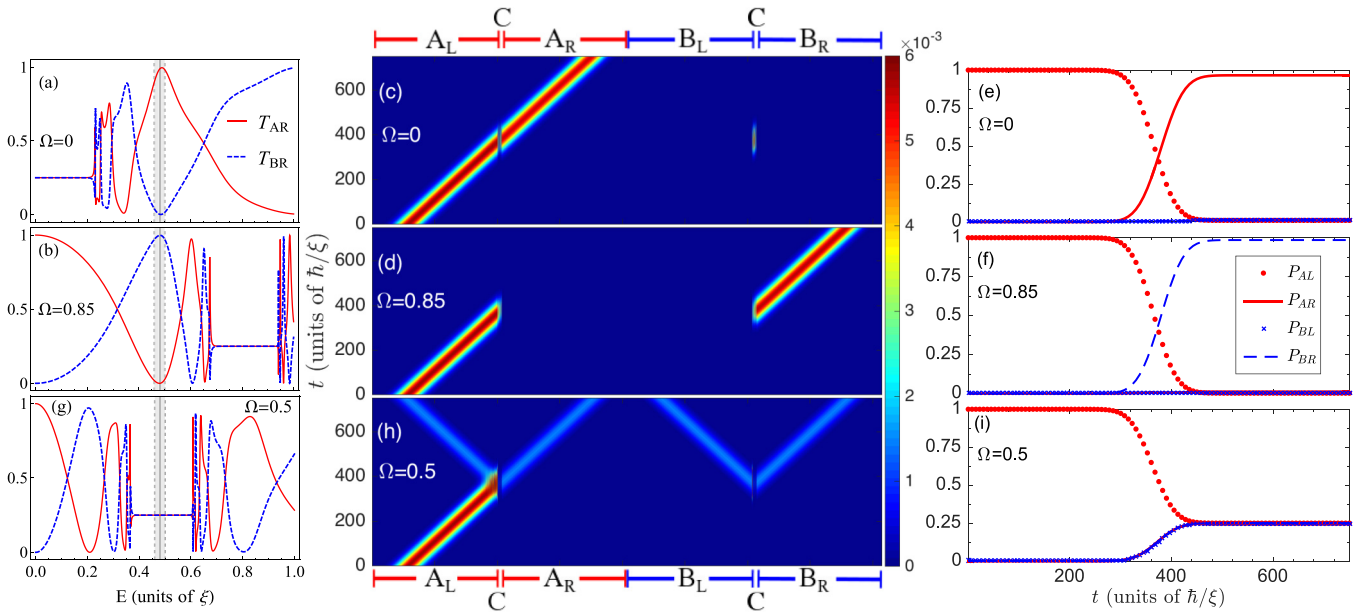

FIG. 2. Left column: stationary spectra of the transmission T_{AR} into the A_R channel (solid red line) and T_{BR} into the B_R channel (dashed blue line). Vertical gray line and shaded areas indicate, respectively, the center position and the width of the initial wave packet used in the dynamics calculation. Middle column: the spatiotemporal map of the wave-packet probability density $|\Psi|^2$; here the waveguide regions are ordered in the following sequence: A_L, C, A_R, B_L, C, B_R. Right column: the probabilities P_{AL} (dotted red line), P_{AR} (solid red line), P_{BL} (blue crosses), and P_{BR} (dashed blue line).

$\Omega = 0$ and $\Omega = 0.85$ is presented in panels (c) and (d) of Fig. 2, respectively. These panels show the spatiotemporal maps of the wave-packet probability density $|\Psi|^2$, manifesting efficient routing. Panels (e) and (f) of Fig. 2 demonstrate the efficiency of the routing at a more quantitative level: they show the dynamics of the integrated probabilities P_{AR} and P_{BR}, whose asymptotic values are swapped between approximately 0.985 and 0.015 when the classical field switches between $\Omega = 0$ and $\Omega = 0.85$. Thus the incident wave packet can be routed almost completely into one or the other right output channel selected by the control field Ω.

To get an insight into the routing mechanism we follow the method used in Ref. [35] to address the same system in the stationary case. Below we present some results which are essential for the explanation of the routing effect (see the latter reference for details). First, we introduce amplitudes in two independent virtual channels: $\Phi_n^{\pm} = \alpha_n \pm \beta_n$. As can be seen from Eq. (2), only the symmetric (+) channel is coupled to the atoms, so the amplitudes Φ_n^{+} account for the scattering and a wave would propagate within the section of the channel with atoms ($1 \leqslant n \leqslant N$) with the renormalized wave vector

$$k_+ = \arccos\left(-\frac{E}{2} + \frac{2\,g^2\,E}{E^2 - \Omega^2}\right). \tag{5}$$

Thus the section with atoms plays a role of an effective potential quantum well or barrier in the symmetric channel. Contrary to that, the antisymmetric channel is decoupled from the atomic states and there is no scattering on atoms in the channel. Amplitudes Φ_n^{-} describe therefore a completely free propagation of a wave with the unperturbed wave vector

$$k_- = k = \arccos\left(-\frac{E}{2}\right). \tag{6}$$

The transmission coefficient in the symmetric channel is given by the following expression [35]:

$$t_+ = \frac{e^{-ikN}\sin k\,\sin k_+}{\sin k\,\sin k_+\cos\left(k_+N\right) + i\left(\cos k\,\cos k_+ - 1\right)\sin\left(k_+N\right)}.$$

As it can be seen from the latter result, if the phases acquired by the wave functions $\Psi^{\pm}$ during their propagation through the section with atoms satisfy

$$k_+N = \pi n_+, \quad k_-N = \pi n_-, \quad n_\pm \in \mathbb{Z}, \tag{7}$$

the transmission coefficient in the symmetric channel becomes $t_+ = \pm 1$ and a wave propagates without reflection. Note that the first condition in Eq. (7) is the condition of the resonant transmission through the virtual energy levels of the effective quantum well or barrier. Both conditions can be met by selecting appropriately the energy E and the field Ω.

If the incoming wave is propagating forward (from left to right) in the channel A_L and the resonance conditions (7) are met, then $\Phi_0^{\pm} = \alpha_0 \pm \beta_0 = \alpha_0$ because the amplitude in the B_L channel $\beta_0 = 0$ (no waves propagate initially in this channel and there are no reflected waves either). Moreover, one can obtain the wave functions in the virtual channels after the scattering (for $n > N$): $\Phi_n^{\pm} \propto \Phi_0^{\pm}\, e^{ik_\pm N} = \alpha_0 e^{i\pi n_\pm}$. Reconstructing wave functions in the real channels we obtain

$$\alpha_n \propto e^{i\pi n_+} + e^{i\pi n_-},$$
$$\beta_n \propto e^{i\pi n_+} - e^{i\pi n_-},$$

from which result it becomes clear that if $n_\pm$ have the same parity, then $\alpha_n \neq 0$ and $\beta_n = 0$ and the transmitted wave remains in the channel A, while if $n_\pm$ are of different parity the wave is routed completely into the channel B: $\alpha_n = 0$ and $\beta_n \neq 0$.

Therefore, the routing effect is determined completely by the constructive or destructive interference of wave functions propagating in virtual channels with and without scattering, which is in a complete analogy with the Fano effect. The important difference from all previous simpler cases is that there are several output channels in our system, so the outcome of the interference is more complex. The outcome can also be controlled by the field Ω, using which an output channel can be selected, in particular.

In the case of a propagating wave packet the above reasoning remains valid if the resonance conditions (7) are satisfied approximately within the energy width of the wave packet; then the packet can be routed almost completely as we have demonstrated.

IV. PULSE SPLITTING

Second, we address the system in the 1/4-splitting regime. As was demonstrated recently [35], the stationary transmission and reflection spectra of the considered system have wide flat subbands in the vicinity of $E = \pm\Omega$. Within these subbands, the probabilities of scattering into the four possible channels (A_L, A_R, B_L, and B_R) are all approximately equal to 1/4 [see panel (g) of Fig. 2 where these characteristics are shown for $\Omega = 0.5$]. Therefore, a propagating wave packet can be split into four approximately equal parts if it is properly centered at $E \approx \pm\Omega$ and its energy width is less than the width of the flat subband(s), which is on the order of $2g = 1$ in our case. The dynamics of such a wave packet with the same parameters as above was calculated for $\Omega = 0.5$. The results are presented in panels (h) and (i) of Fig. 2, which show an even splitting of the incident wave packet. In particular, panel (i) shows that the asymptotic values of all probabilities are equal, $P_{AL,AR} = P_{BL,BR} = 0.25$, indicating that the incident wave packet is split in four equal parts.

To understand the mechanism of such an even splitting, we plot in Fig. 3(a) the dynamics of the probability densities $|u_j|^2$ and $|v_j|^2$, which shows clearly that only the states of the leftmost atom (with $j = 1$) are excited during the pulse scattering, suggesting that the whole extended junction operates as a point scattering defect. For comparison, Fig. 3(b) shows the dynamics in the routing mode in which all atoms of the junction are excited. The former finding confirms our earlier stationary result [35]: within the 1/4-scattering flat bands, the entire junction acts as a very high quantum-mechanical barrier. The latter can be seen from Eq. (5): when $|E - \Omega| \ll g^2$ the wave vector k_+ becomes imaginary and large: $|k_+| \gg 1$. In this case the wave-function amplitude in the symmetric channel decays exponentially under the barrier (in the section with atoms): $\Phi_n^+ \propto e^{-|k_+|(n-1)}$ for $1 \leqslant n \leqslant N$. Because the atomic states are coupled to the symmetric channel, the wave function at the atoms also decays exponentially and becomes negligible already at the second atom. Note that the wave function on the sites adjacent to the atoms is not small due to the contribution of the antisymmetric channel: $\alpha_n \approx -\beta_n \approx \Phi_n^-$ for $n > 1$. Thus the whole atomic section acts as an effective isotropic point scatterer and splits the incoming wave packet into approximately four equal parts. On the other hand, in the single-photon regime, such a system can be used as a quantum random number generator (some proposals of such devices can be found in Refs. [37,38]): each mutually exclusive single-photon detection in either of the four channels would give a two-bit random number. Moreover, given that the 1/4-scattering band is wide, several photons with different, yet experimentally distinguishable, energies (within the band) can be sent in parallel to generate a higher bit depth random number.

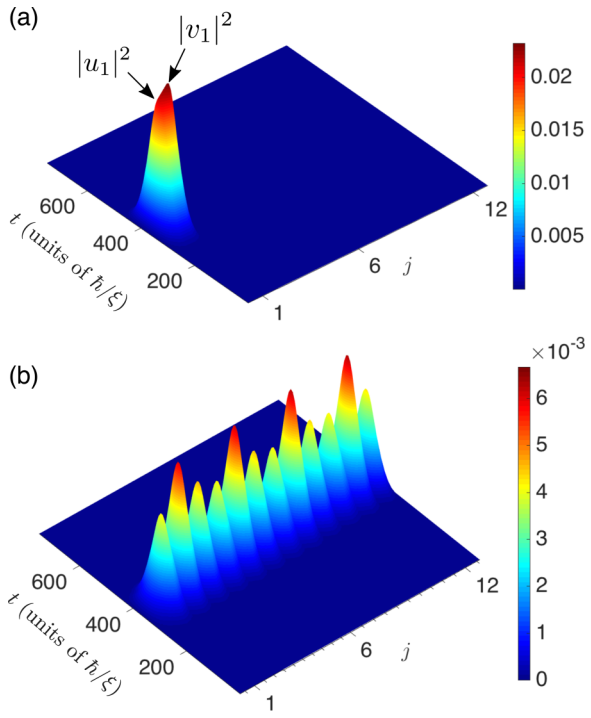

FIG. 3. Dynamics of the probability densities at the atomic states $|e_j\rangle$ and $|s_j\rangle$ depicted in pairs: $\{|u_j|^2, |v_j|^2\}$ ($j = 1 \ldots 12$). The results are calculated for the splitting mode (upper panel) and the controlled routing mode (lower panel). All parameters are the same as for the lower and the middle row of Fig. 2, respectively.

V. PULSE DELAY AND STORAGE

Next, to address the delay and storage properties of the quantum junction, we simulate the propagation of the wave packet with $\sigma = 100$ and $k_0 = \pi/2$. Figure 4 presents results of such calculations for $\Omega = 0.12$ in the upper row and those for $\Omega = 0.08$ in the lower row. The left column of Fig. 4 displays the spatiotemporal map of the wave-packet probability density $|\Psi|^2$, while the middle column shows the dynamics of probabilities $P_{AL,AR}$, $P_{BL,BR}$, and P_C. These plots demonstrate that, when the wave packet (incoming from the A_L channel) reaches the junction, it is partially scattered into the two right output channels A_R and B_R. As a result, two almost identical *primary* scattered pulses start propagating freely in the output channels [these pulses are labeled by p in Figs. 4(a) and 4(b)]. Each of these two pulses carries about 1/4 of the probability; the remaining 1/2 of the probability is stored in the atomic states as can be seen from panel (c) of Fig. 4 for $400 \lesssim t \lesssim 500$ (see the green dash-dotted line). Panels (a) and (c) of Fig. 4 show also that two *secondary* pulses start propagating in the two right output channels after some delay [those pulses are labeled by s in Fig. 4(a)]. Those *secondary*

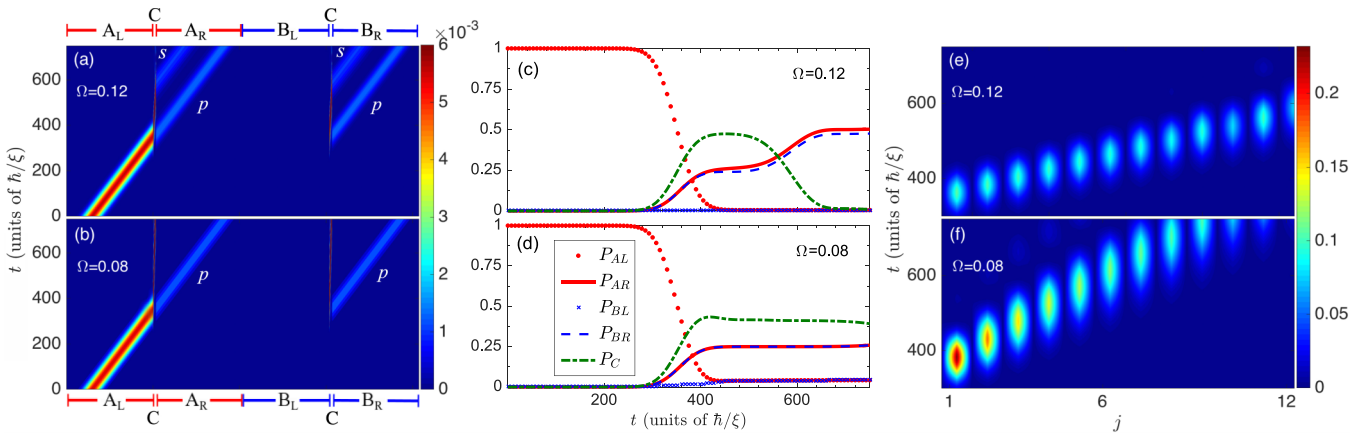

FIG. 4. Left column: the spatiotemporal map of the wave-packet probability density $|\Psi|^2$. The *primary* and *secondary* pulses are labeled by p and s, respectively. The middle column shows the probabilities P_{AL} (dotted red line), P_{AR} (solid red line), P_{BL} (blue crosses), P_{BR} (dashed blue line), and P_C (green dash-dotted line). Right column: the dynamics of the probability densities at the states $|e_j\rangle$ and $|s_j\rangle$ depicted in pairs $\{|u_j|^2,\ |v_j|^2\}$ $(j = 1 \ldots 12)$.

pulses are broadened with respect to the *primary* ones but they also carry about $1/4$ of the probability each [see Fig. 4(c)].

To get an insight in the mechanisms of the *secondary* pulse formation and delay we plot in the right column of Fig. 4 the spatiotemporal maps of the probability densities $|u_j|^2$ and $|v_j|^2$ at the atomic states $|e_j\rangle$ and $|s_j\rangle$, respectively. The two maps show that the incident pulse is forming the *secondary* one, which is propagating in the junction over the atomic $|s_j\rangle$ states (note that $|u_j|^2 = 0$). While such a *secondary* pulse is propagating in the junction, it has a considerably smaller group velocity than those pulses propagating freely in the input-output channels. The group velocity is small because the $|s_j\rangle$ states are coupled indirectly via the waveguide states and the excited $|e_j\rangle$ states. The $|s_j\rangle$ and $|e_j\rangle$ states are coupled by the field Ω and, therefore, it is natural to expect that the smaller group velocity depends on the magnitude of the control field Ω which determines this coupling.

After some algebra, the stationary Hamiltonian in the right-hand side of Eq. (1) can be diagonalized and group velocities can be obtained for the states that are close to the center of the band ($k = \pi/2$, $E = 0$). There are two types of eigenfunctions with zero energy. One type is free propagating waves decoupled from the atoms and having the group velocity $v_g = 2$ [which is the same as that of the plane waves with the dispersion relation $E(k) = -2\cos k$]. On the other hand, there are eigenstates that have the following structure in the section with atoms ($j = 1 \ldots N$):

$$\alpha_j = -1 - \frac{\Omega^2}{g^2}, \quad \beta_j = 1, \quad u_j = 0, \quad v_j = \frac{\Omega}{g}. \tag{8}$$

Given that $u_j = 0$, these states are decoupled from the "bright" excited states $|e_j\rangle$, while they have a contribution of the "dark" states $|s_j\rangle$; such states are analogous to the dark polaritonic states discussed in Ref. [39]. The corresponding group velocity

$$v_g = \frac{2\,\Omega^2}{2\,g^2 + \Omega^2} \tag{9}$$

is reduced considerably with respect to that of the free propagation if $\Omega/g \ll 1$. Therefore, the part of the wave packet, which is stored in these dark states can be delayed compared to its free propagating counterpart. Such a delay has also been predicted from the analysis of phases of the stationary transmission coefficients [40].

Panels (e) and (f) of Fig. 4 confirm the above reasoning, showing that the group velocity decreases with the coupling field (note the difference in the slopes of the spatiotemporal dynamics). When the slow *secondary* pulse reaches the right extreme of the junction, it scatters into the two right output channels, forming two almost identical broadened *secondary* pulses which propagate freely with the group velocity $v_g = 2$ in A_R and B_R channels following the *primary* pulses. Because of the above-mentioned difference in the group velocities, the *secondary* pulse is delayed with respect to the *primary* one. As we have argued, this delay can be tuned by the classical field Ω, which suggests a mechanism of the pulse delay control.

Note also that, when the incident pulse has already scattered into the output channels in the form of the *primary* pulses, the *secondary* pulse can still be propagating in the junction over its atomic states $|s_j\rangle$. If the control field Ω is switched off at such a moment, the *secondary* pulse can be "frozen" or stored in the atomic states $|s_j\rangle$ because they would be completely decoupled from the states $|e_j\rangle$ and the rest of the system. Within our idealized model (which neglects dissipation completely), such storage has an unlimited time: the stored part of the wave function preserves its amplitudes at the atomic states and relative phases. Then, if the external field is switched back on, the stored pulse would be "released" and continue its propagation, suggesting a pulse trapping or storage control mechanism.

VI. DISSIPATION EFFECTS

Finally, we study the impact of dissipation on the operation properties of our proposed device. Dissipation in the waveguides would only gradually reduce the probability density of the propagating pulses. Therefore, the latter effect is trivial

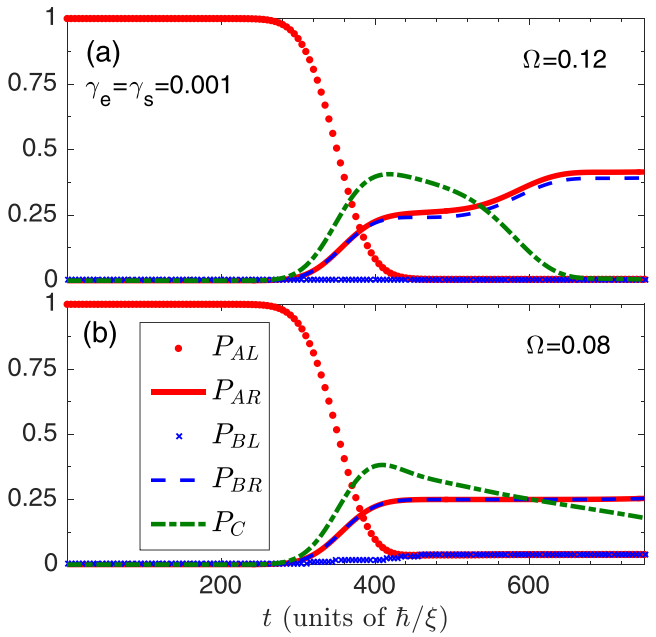

FIG. 5. Dynamics of the probabilities P_{AL} (dotted red line), P_{AR} (solid red line), P_{BL} (blue crosses), P_{BR} (dashed blue line), and P_C (green dash-dotted line) calculated for the same values of Ω as in Fig. 4 and decay rates $\gamma_e = \gamma_s = 0.001$

and we neglect the corresponding dissipation for clarity. In order to address the dissipation within the junction, we use the standard method introducing the phenomenological decay rates γ_e and γ_s of the atomic states $|e_j\rangle$ and $|s_j\rangle$, respectively. This method has been used for similar systems (see Refs. [10,14,41–43]). Within this approach the frequencies ω_e and ω_s are substituted by $\omega_e' = \omega_e - i\gamma_e$ and $\omega_s' = \omega_s - i\gamma_s$, respectively. Hereafter we use $\gamma_e = \gamma_s = 0.001$, following Refs. [14,41,44].

We found that the impact of the considered dissipation on the controlled routing and 1/4-splitting properties was negligible. For example, in the routing regime, the asymptotic probability P_{BR} decreases by only 1.5% for $\Omega = 0.85$. In the splitter regime, the asymptotic probabilities decrease only in the left channels by about 0.4%. Therefore, both regimes are robust to low dissipation.

Figure 5 displays the dynamics of probabilities $P_{AR,AL}$, $P_{BR,BL}$, and P_C for the dissipative case. These results show that the considered low decays in the atomic states do not affect the propagation of the *primary* pulses at all because the latter propagates freely in the output channels A_R and B_R [35]. Each of these pulses carries about 0.25 of the total probability: see solid red and dashed blue lines in Fig. 5 for $400 \lesssim t \lesssim 500$ (which can be compared to their counterparts in the nondissipative case shown in Fig. 4). On the other hand, when the *secondary* pulse propagates in the quantum junction, it propagates mostly over the atomic states $|s_j\rangle$ [see panels (e) and (f) of Fig. 4]. Due to the decay in these states, a part of the probability dissipates, causing a corresponding decrease of the integrated probabilities of the *secondary* pulses in A_R and B_R channels. For example, for $\Omega = 0.12$ the asymptotic values of P_{AR} and P_{BR} decrease by approximately 0.1 each, as compared with the nondissipative case. Such a decrease is in good agreement with the simple estimate which assumes that about $1 - \exp(-\gamma_s \tau)$ of the probability is dissipated, where τ is the *secondary* pulse delay time ($\tau \sim 200$ for $\Omega = 0.12$). Given that the group velocity of the *secondary* pulse in the quantum junction decreases with the control field Ω [compare panels (e) and (f) of Fig. 4], the effect of losses in the model is more pronounced for smaller values of Ω due to the fact that the pulse delay is longer and the pulse spends more time in the decaying $|s_j\rangle$ states. We note finally that the decay of the $|e_j\rangle$ states is not as important because the amplitude of the wave function on these states is negligible in the considered regime; therefore, γ_e can be substantially larger without affecting the properties of the device, as long as γ_s is small enough.

VII. CONCLUSIONS

In conclusion, we studied the dynamics of optical pulses in the system of two waveguides coupled by the multipurpose quantum junction comprising a set of three-level atoms with the Λ scheme of the optical transitions, one of which is driven by an external classical electromagnetic control field. We demonstrate that photonic wave packets propagating in the system can be controlled and manipulated in various ways. In particular, an incident pulse can be routed into a selected output channel or split into several parts, some of which can be delayed by an amount of time determined by the control field. The pulse can also be partially trapped or stored in the junction and released afterward in a controlled way. Moreover, the same physical device can perform all these operations with high efficiency. The system's operational regimes have been shown to be robust in the presence of low dissipation of the atomic states. Therefore, we argue that our proposed model system can provide helpful guidelines for designing the multifunctional junctions, making the future all-optical circuitry building blocks more multipurpose and integrated. Furthermore, since our model is simple and quite generic, similar devices can be designed based not only on atomic but also on other physical three-level systems, such as SQUIDs (superconducting quantum interference devices). We believe that the wide variety of operational regimes combined with high operation efficiency makes our model design a promising prototype for applications in next-generation information processing and communication technologies.

ACKNOWLEDGMENTS

Work in Madrid was supported by MINECO Grant No. MAT2016-75955. M.A. and P.A. acknowledge financial support from DGIIP UTFSM and ANID FONDECYT Grants No. 1180914 and No. 1201876. M.A. also acknowledges support from ANID Doctorado Nacional through Grant No. 21141185 and J. F. Marín for fruitful discussions. A.M. is grateful to V. A. Malyshev for critical discussions.

[1] H. J. Kimble, Nature (London) **453**, 1023 (2008).

[2] T. E. Northup and R. Blatt, Nat. Photon. **8**, 356 (2014).

[3] C. Monroe, Nature (London) **416**, 238 (2002).
[4] T. D. Ladd, F. Jelezko, R. Laflamme, Y. Nakamura, C. Monroe, and J. L. O'Brien, Nature (London) **464**, 45 (2010).
[5] S. Ritter, C. Nölleke, C. Hahn, A. Reiserer, A. Neuzner, M. Uphoff, M. Mücke, E. Figueroa, J. Bochmann, and G. Rempe, Nature (London) **484**, 195 (2012).
[6] F. Flamini, N. Spagnolo, and F. Sciarrino, Rep. Prog. Phys. **82**, 016001 (2018).
[7] J. L. O'Brien, A. Furusawa, and J. Vučković, Nat. Photon. **3**, 687 (2009).
[8] A. Reiserer and G. Rempe, Rev. Mod. Phys. **87**, 1379 (2015).
[9] L. Zhou, Z. R. Gong, Y.-x. Liu, C. P. Sun, and F. Nori, Phys. Rev. Lett. **101**, 100501 (2008).
[10] Z. R. Gong, H. Ian, L. Zhou, and C. P. Sun, Phys. Rev. A **78**, 053806 (2008).
[11] Y. Chen, M. Wubs, J. Mørk, and A. F. Koenderink, New J. Phys. **13**, 103010 (2011).
[12] L. Zhou, L.-P. Yang, Y. Li, and C. P. Sun, Phys. Rev. Lett. **111**, 103604 (2013).
[13] J. Lu, L. Zhou, L.-M. Kuang, and F. Nori, Phys. Rev. A **89**, 013805 (2014).
[14] J.-S. Huang, J.-W. Wang, Y. Wang, Y.-L. Li, and Y.-W. Huang, Quantum Inf. Process. **17**, 78 (2018).
[15] J.-S. Huang, J.-W. Wang, Y. Wang, and Y.-W. Zhong, J. Phys. B: At., Mol., Opt. Phys. **51**, 025502 (2018).
[16] J. Lu, Z. H. Wang, and L. Zhou, Opt. Express **23**, 22955 (2015).
[17] L. Liu and J. Lu, Quantum Inf. Process. **16**, 29 (2016).
[18] T. Aoki, A. S. Parkins, D. J. Alton, C. A. Regal, B. Dayan, E. Ostby, K. J. Vahala, and H. J. Kimble, Phys. Rev. Lett. **102**, 083601 (2009).
[19] K. Xia and J. Twamley, Phys. Rev. X **3**, 031013 (2013).
[20] I. Shomroni, S. Rosenblum, Y. Lovsky, O. Bechler, G. Guendelman, and B. Dayan, Science **345**, 903 (2014).
[21] X. Li, W.-Z. Zhang, B. Xiong, and L. Zhou, Sci. Rep. **6**, 39343 (2016).
[22] C. Cao, Y.-W. Duan, X. Chen, R. Zhang, T.-J. Wang, and C. Wang, Opt. Express **25**, 16931 (2017).
[23] W.-B. Yan and H. Fan, Sci. Rep. **4**, 4820 (2014).
[24] C.-H. Yan, Y. Li, H. Yuan, and L. F. Wei, Phys. Rev. A **97**, 023821 (2018).
[25] I.-C. Hoi, C. M. Wilson, G. Johansson, T. Palomaki, B. Peropadre, and P. Delsing, Phys. Rev. Lett. **107**, 073601 (2011).
[26] X. X. Yuan, J.-J. Ma, P.-Y. Hou, X.-Y. Chang, C. Zu, and L.-M. Duan, Sci. Rep. **5**, 12452 (2015).
[27] C. Y. Hu, Sci. Rep. **7**, 45582 (2017).
[28] J.-H. Kim, S. Aghaeimeibodi, C. J. K. Richardson, R. P. Leavitt, and E. Waks, Nano Lett. **18**, 4734 (2018).
[29] F. Morichetti, C. Ferrari, A. Canciamilla, and A. Melloni, Laser Photon. Rev. **6**, 74 (2012).
[30] M. Notomi, E. Kuramochi, and T. Tanabe, Nat. Photon. **2**, 741 (2008).
[31] H. Takesue, N. Matsuda, E. Kuramochi, W. J. Munro, and M. Notomi, Nat. Commun. **4**, 2725 (2013).
[32] N. Matsuda, E. Kuramochi, H. Takesue, and M. Notomi, Opt. Lett. **39**, 2290 (2014).
[33] S. Mookherjea, J. S. Park, S.-H. Yang, and P. R. Bandaru, Nat. Photon. **2**, 90 (2008).
[34] M. Hartmann, F. Brandão, and M. Plenio, Laser Photon. Rev. **2**, 527 (2008).
[35] M. Ahumada, P. A. Orellana, F. Domínguez-Adame, and A. V. Malyshev, Phys. Rev. A **99**, 033827 (2019).
[36] Note that this Hamiltonian is different from those in some earlier works due to differences in the used rotating frames.
[37] M. Herrero-Collantes and J. C. Garcia-Escartin, Rev. Mod. Phys. **89**, 015004 (2017).
[38] M. Gräfe, R. Heilmann, A. Perez-Leija, R. Keil, F. Dreisow, M. Heinrich, H. Moya-Cessa, S. Nolte, D. N. Christodoulides, and A. Szameit, Nat. Photon. **8**, 791 (2014).
[39] M. Fleischhauer and M. D. Lukin, Phys. Rev. Lett. **84**, 5094 (2000).
[40] M. Ahumada, Ph.D. thesis, Universidad Técnica Federico Santa María, 2021.
[41] J.-S. Huang, J.-W. Wang, Y.-L. Li, Y. Wang, and Y.-W. Huang, Quantum Inf. Process. **18**, 59 (2019).
[42] Y. Chang, Z. R. Gong, and C. P. Sun, Phys. Rev. A **83**, 013825 (2011).
[43] M.-T. Cheng, X.-S. Ma, M.-T. Ding, Y.-Q. Luo, and G.-X. Zhao, Phys. Rev. A **85**, 053840 (2012).
[44] P. Samutpraphoot, T. Đorđević, P. L. Ocola, H. Bernien, C. Senko, V. Vuletić, and M. D. Lukin, Phys. Rev. Lett. **124**, 063602 (2020).